

---

Faculty Scholarship

---

5-19-2022

## Extrusion: A New Method for Rapid Formulation of High-Yield, Monodisperse Nanobubbles

Claire Council

*Case Western Reserve University, [claire.council@case.edu](mailto:claire.council@case.edu)*

Eric Abenojar

*Case Western Reserve University, [eric.abenojar@case.edu](mailto:eric.abenojar@case.edu)*

Reshani Perera

*Case Western Reserve University, [reshani.perera@case.edu](mailto:reshani.perera@case.edu)*

Agata A. Exner

*Case Western Reserve University, [agata.exner@case.edu](mailto:agata.exner@case.edu)*

Author(s) ORCID Identifier:

[Claire Council](#)

[Eric Abenojar](#)

[Reshani Perera](#)

[Agata A. Exner](#)

Follow this and additional works at: <https://commons.case.edu/facultyworks>

Digital Part of the [Radiology Commons](#)  
Commons

---

Network

### Recommended Citation

Council, C., Abenojar, E., Perera, R., Exner, A. A., Extrusion: A New Method for Rapid Formulation of High-Yield, Monodisperse Nanobubbles. *Small* 2022, 18, 2200810. <https://doi.org/10.1002/smll.202200810>

This Article is brought to you for free and open access by Scholarly Commons @ Case Western Reserve University. It has been accepted for inclusion in Faculty Scholarship by an authorized administrator of Scholarly Commons @ Case Western Reserve University. For more information, please contact [digitalcommons@case.edu](mailto:digitalcommons@case.edu).

CWRU authors have made this work freely available. [Please tell us](#) how this access has benefited or impacted you!

# Extrusion: A New Method for Rapid Formulation of High-Yield, Monodisperse Nanobubbles

Claire Counil, Eric Abenojar, Reshani Perera, and Agata A. Exner\*

Shell-stabilized gas microbubbles (MB) and nanobubbles (NB) are frequently used for biomedical ultrasound imaging and therapeutic applications. While it is widely recognized that monodisperse bubbles can be more effective in these applications, the efficient formulation of uniform bubbles at high concentrations is difficult to achieve. Here, it is demonstrated that a standard mini-extruder setup, commonly used to make vesicles or liposomes, can be used to quickly and efficiently generate monodisperse NBs with high yield. In this highly reproducible technique, the NBs obtained have an average diameter of  $0.16 \pm 0.05 \mu\text{m}$  and concentration of  $6.2 \pm 1.8 \times 10^{10}$  NBs  $\text{mL}^{-1}$  compared to  $0.32 \pm 0.1 \mu\text{m}$  and  $3.2 \pm 0.7 \times 10^{11}$   $\text{mL}^{-1}$  for NBs made using mechanical agitation. Parameters affecting the extrusion and NB generation process including the temperature, concentration of the lipid solution, and the number of passages through the extruder are also examined. Moreover, it is demonstrated that extruded NBs show a strong acoustic response *in vitro* and a strong and persistent US signal enhancement under nonlinear contrast enhanced ultrasound imaging in mice. The extrusion process is a new, efficient, and scalable technique that can be used to easily produce high yield smaller monodispersed nanobubbles.

vary according to the viscoelasticity of the shell, the type of gas, the size of the bubbles and also the surrounding environment. Lipid-shelled nanobubbles (NBs) with a fluorocarbon (FC) gas core are a promising new generation of therapeutic agents for both ultrasound contrast imaging and controlled drug delivery applications.<sup>[3–10]</sup> Clinically-used ultrasound contrast agents (UCAs) (1–10  $\mu\text{m}$  MBs) are limited to intravascular applications, while NBs, because of their size, can extravasate out of the vasculature and into the tumor tissue.<sup>[11]</sup> This property makes it possible to use NBs for cancer therapeutic applications such as ultrasound image-guided surgeries and biopsies, tumor characterization, cell targeting, as well as ultrasound triggered and targeted drug delivery.<sup>[11–19]</sup> A formulation of NBs developed recently in our group has led to improvement in NB stability *in vitro* and *in vivo*.<sup>[20,21]</sup> These NBs are more resistant to deformation due to the incorporation of

## 1. Introduction

Microbubble (MB) ultrasound contrast agents have been clinically utilized over the past >20 years. After the initial discoveries made nearly 50 years ago showing quickly-dissipating ultrasound signal generated from air bubbles *in vivo*<sup>[1]</sup> several subsequent generations of MBs have improved their stability by adding a lipid, polymer, or protein shell and using a hydrophobic gas (such as perfluoropropane  $\text{C}_3\text{F}_8$  or sulfur hexafluoride  $\text{SF}_6$ ) for the core. Bubbles generate ultrasound contrast by oscillation in response to positive and negative pressure changes under an acoustic field.<sup>[2]</sup> The response can

glycerol (Gly), a membrane stiffener known to increase buckling of lipid monolayers and addition of propylene glycol (PG), an edge-activator used in ultradeformable liposomal formulations, which imparts flexibility to the NB shell (Figure 1).<sup>[22–26]</sup> These components can be manipulated to obtain shells of varying viscoelastic properties, which can then be used to modulate bubble response in an acoustic field. For example, a recent publication described a pressure-dependent response of the NBs with three different shells.<sup>[27]</sup> However, the effects were only apparent when the NBs population was filtered to reduce the polydispersity of NB size.

Size distribution is a known critical factor contributing to the bubble acoustic response. Reducing the polydispersity of bubbles results in more uniform nonlinear behavior and increased signal to noise ratio. The amplified activity increases the sensitivity of detection and bubble response at a specific pressure, which in turn, can lead to improvement in molecular imaging and drug delivery applications. These effects are predicted theoretically, and have been demonstrated experimentally, *in vitro* and *in vivo*.<sup>[28]</sup> However, most current formulation methods used for production of NBs and MBs, do not yield a uniform bubble size. The most common techniques used are mechanical agitation,<sup>[20]</sup> sonication,<sup>[29]</sup> and microfluidic assembly.<sup>[30–32]</sup> For isolating NBs, a repurposed dental amalgamator (Vialmix) has been frequently used to force shell self-assembly around the gas core, followed by filtration or differential centrifugation to

C. Counil, E. Abenojar, R. Perera, A. A. Exner  
Department of Radiology  
Case Western Reserve University  
10900 Euclid Avenue, Cleveland, OH 44106-7207, USA  
E-mail: agata.exner@case.edu

 The ORCID identification number(s) for the author(s) of this article can be found under <https://doi.org/10.1002/sml.202200810>.

© 2022 The Authors. Small published by Wiley-VCH GmbH. This is an open access article under the terms of the Creative Commons Attribution License, which permits use, distribution and reproduction in any medium, provided the original work is properly cited.

DOI: 10.1002/sml.202200810

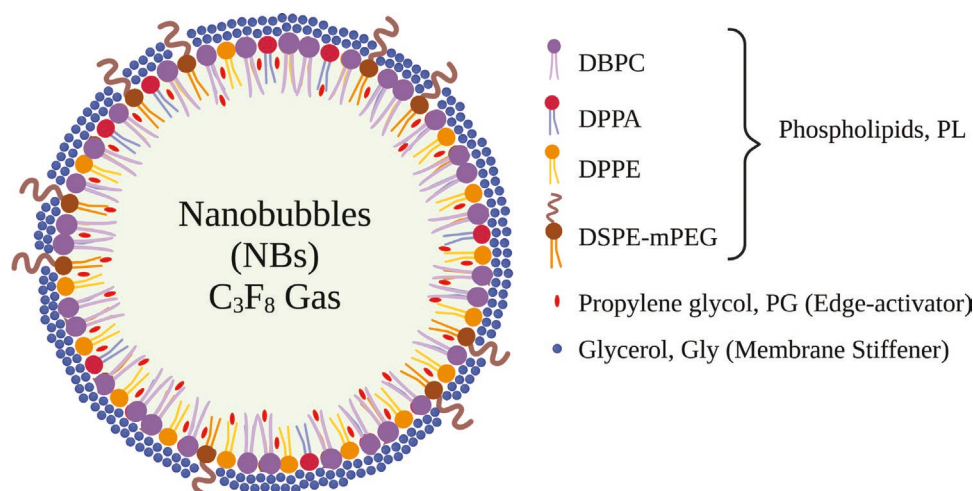


**Figure 1.** Schematic representation of the nanobubble shell structure and composition. The shell is composed of 4 different phospholipids: DBPC, DPPA, and DPPE and mPEG(2k)-DSPE at a weight ratio of 6:1:2:1. To help NB stability and the acoustic response, propylene glycol (PG) and glycerol (Gly) were used as edge-activator and membrane stiffener, respectively, as previously<sup>[27]</sup> (Created with BioRender).

remove MBs.<sup>[20]</sup> This process is inefficient and discards >50% of lipids utilized in the starting material. It also results in relatively polydisperse bubbles. Sonication also produces bubbles with a broad size distribution. While rapid MB assembly is effective with microfluidics, and new improvements have increased the production efficiency,<sup>[33]</sup> the process is yet untested for NBs and requires specialized equipment.

Here, we present for the first time, an alternative highly efficient technique for nanobubble formulation using a commercially available miniextruder setup.<sup>[25]</sup> The principle behind this system is to pass a dispersion of lipids (one or a mixture) several times through a porous membrane to arrive at a dispersion of monodispersed vesicles/liposomes. The formation of the vesicles/liposomes is made possible by extrusion, if the processes take place at a temperature higher than their phase transition temperature such that the lipids are in a fluid state.<sup>[34–37]</sup> While commonly utilized as a strategy for formulating liposomes, to our knowledge, the work presented here is the first to demonstrate the ability to form stable monodisperse gas-core nanostructures using the mini-extruder system.

This paper first presents a comparison of NBs obtained using two different methods: a) using mechanical agitation (Vialmix) to generate the bubbles followed by differential centrifugation (v-NBs) and b) using extrusion to form NBs and centrifugation to remove the foam (e-NBs). The NBs were characterized and compared with regard to size, concentration, yield, and nonlinear acoustic response. Our results show that the extrusion method produces a yield that is at least 5 times higher in volume, with a similar quantity of bubbles when 49% less PL is used initially compared to the control method. The extrusion method presented here also produced smaller ( $\approx 160$  vs  $\approx 320$  nm) and more monodisperse (full width at half maximum, FWHM, of 190 nm versus 113 nm) NBs without drastically impacting the acoustical response of the agents. In the second part of the paper, three parameters that can be modified and optimized on the extruder process were investigated: a) the temperature of extrusion, b) the concentration

of the lipid solution, and c) the number of passes through the extruder. The effect of these parameters were studied to show how each can interfere and influence NB formation by the extrusion process. Finally, we present an *in vivo* experiment with e-NBs lightly modified in terms of size isolation. The final e-NBs provided similar initial response as v-NBs and a stable signal up to 10 min.

## 2. Results and Discussion

Mechanical agitation (via Vialmix),<sup>[20]</sup> sonication, and microfluidic devices<sup>[30]</sup> are well-known techniques used to obtain nano and microbubbles. On the other hand, mini-extruders are commonly used to produce monodisperse vesicles and liposomes.<sup>[38–40]</sup> This instrument consists of a polycarbonate membrane placed in between two filters sealed by two O-rings made of Teflon. Passing a phospholipid solution several times through this membrane at a temperature higher than the transition temperature of the PL induces the formation of monodisperse vesicles. However, we found that the potential use of mini-extruders is not only limited to the formation of liquid core self-assembly but can also be extended to produce gas core vesicles, such as NBs. The NBs obtained with this new technique have been characterized and compared to those commonly produced in our group using a mechanical agitation<sup>[20]</sup> with regard to size, concentration, ultrasound response, and signal decay rate.

### 2.1. Extruder versus Mechanical Agitation

The mechanical agitation and extruder methods produced NB solutions with different characteristics (**Figure 2**) as determined by resonant mass measurement (RMM).<sup>[41]</sup> With the standard mechanical agitation via Vialmix (v-NB), 0.5 mL of NBs at a concentration of  $3.2 \pm 0.7 \times 10^{11}$  v-NBs mL<sup>-1</sup> were obtained (**Figure 2A,C**), with a mean diameter of  $0.32 \pm 0.1 \mu\text{m}$

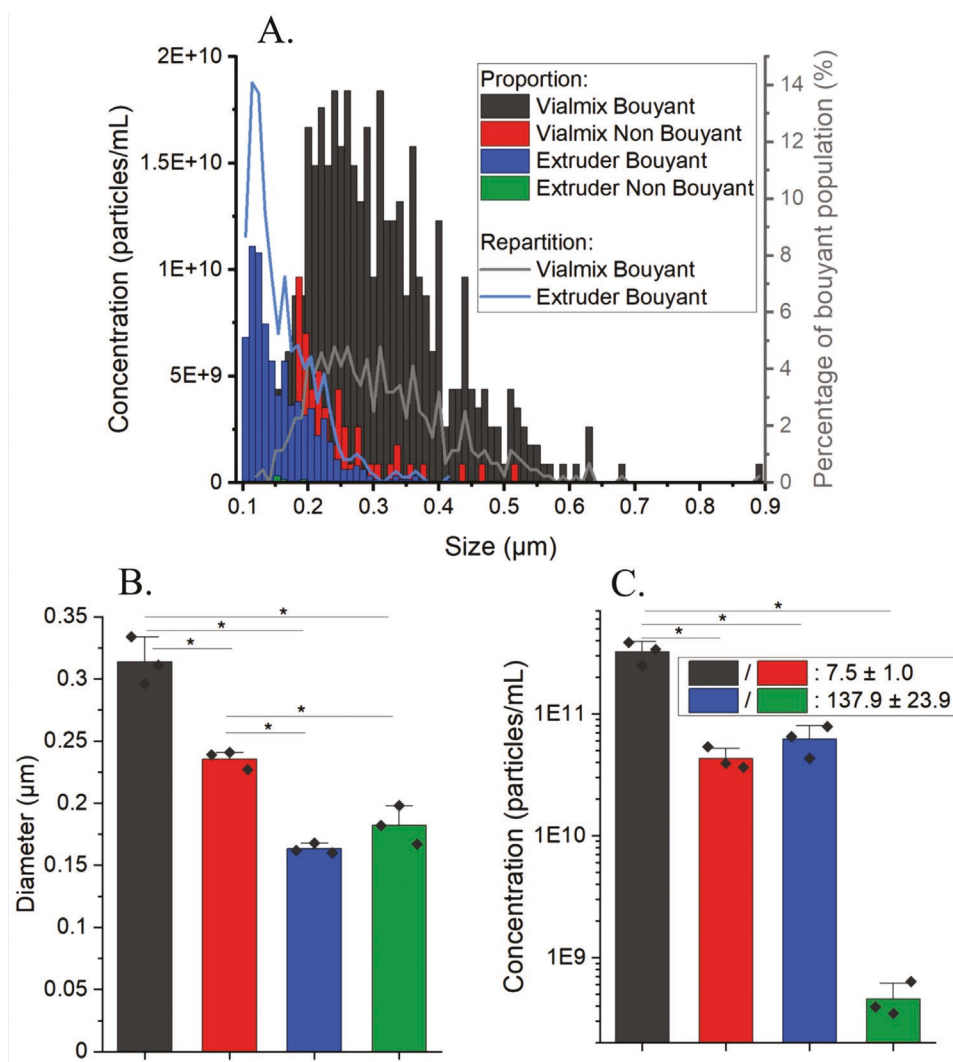


**Figure 2.** Physical characterization of v-NBs and e-NBs using resonant mass measurement: A) Buoyant and nonbuoyant particle size and concentration distribution. B) Mean nanobubble diameter, and C) Total concentration of buoyant and nonbuoyant particles. Asterisk indicates significant difference at  $p < 0.05$ .

for each trial according to the RMM with  $\pm 0.02 \mu\text{m}$  variation of the mean radius between the 3 measurements (Figure 2B). With the extruder (e-NB), a higher volume of solution was obtained, between 2.5 and 3 mL at a concentration at  $6.2 \pm 1.8 \times 10^{10}$  e-NBs  $\text{mL}^{-1}$  (Figure 2C). The mean diameter was reduced to  $0.16 \pm 0.05 \mu\text{m}$  for each trial according to the RMM with a  $\pm 0.004 \mu\text{m}$  variation of the mean radius between the 3 measurements (Figure 2B). The extruder provided more monodisperse and more reproducible NBs samples. The minimum volume obtained with the mini-extruder (2.5 mL) provided the same quantity of bubbles as mechanical agitation:  $1.6 \times 10^{11}$  NBs using 49% less of the starting phospholipid mixture. Moreover, the mini-extruder produced e-NBs that were more monodisperse as demonstrated by a Full Width at Half Maximum (FWHM) of 0.113 versus 0.190  $\mu\text{m}$  for v-NBs solution, and a smaller size range with e-NBs having bubble size distribution between 0.1 and 0.4  $\mu\text{m}$  e-NBs in comparison to 0.2–1  $\mu\text{m}$  for v-NBs (Figure 2A). All the bins of v-NBs population represent less than 5% of the total concentration of the

NBs. However for e-NBs all the bins between 0.1 and 0.2  $\mu\text{m}$  had a percentage higher than 4%, and between 0.104 and 0.144 is even higher than 8% (Figure 2A), further confirming that the mini-extruder produced more monodisperse agents.

In addition, using the extruder for NB formulation produced proportionally fewer nonbuoyant particles in the sample. The ratio for buoyant (bubbles) to nonbuoyant particles was 8:1 for v-NBs compared to 138:1 for e-NBs (Figure 2C). This result from e-NBs was unexpected considering the main use of the mini-extruder method is for the production of nonbuoyant particles. These results show that the mini-extruder is a powerful technique for the formulation of a high yield monodisperse populations of NBs with a diameter lower than 200 nm.

The size of the NBs obtained with RMM was also compared to those obtained using transmission electron microscopy (TEM) imaging analysis (Figure 3). As expected, the mini-extruder generates significantly smaller NBs compared to the mechanical agitation method. The white rod like structure observed in the e-NBs likely correspond to the salt crystals

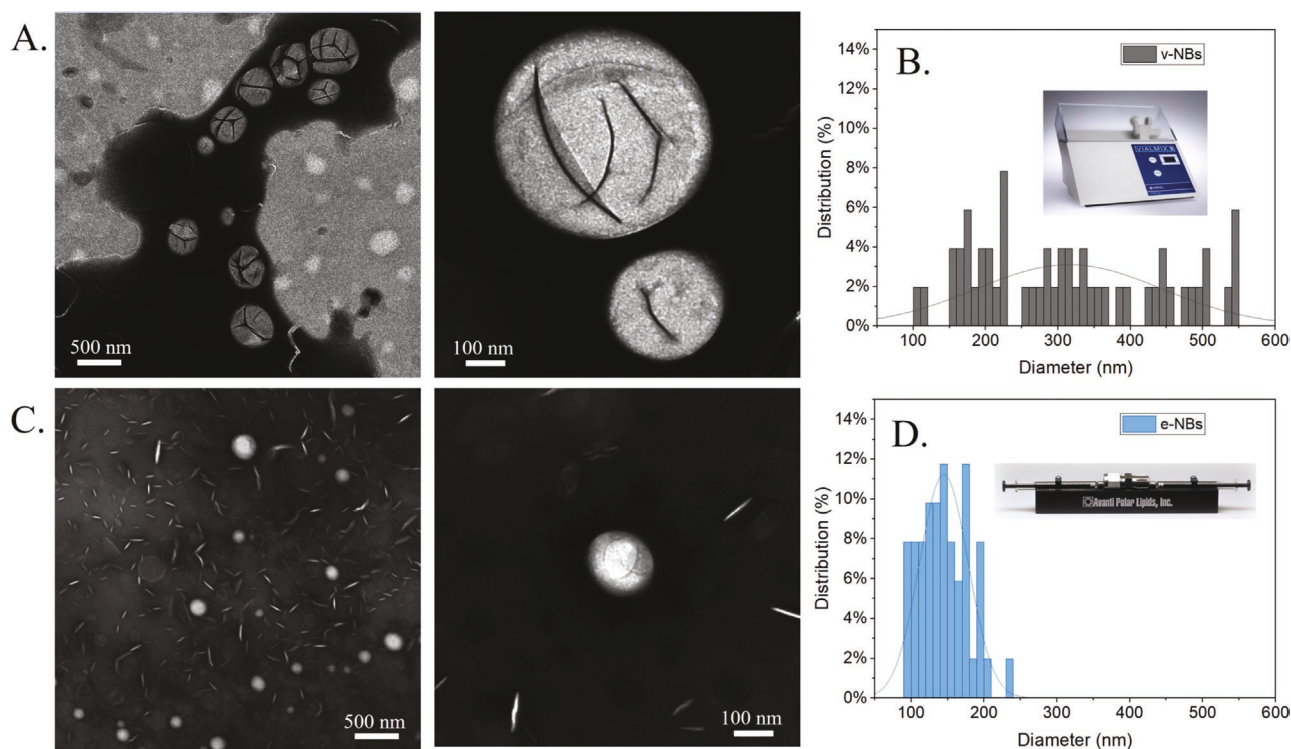


**Figure 3.** TEM images of A) v-NBs and C) e-NBs and distribution of size of B) v-NBs and D) e-NBs on 50 particles.

from phosphate buffer saline (PBS). The crystals are less visible in v-NBs because of lower concentration (Figure 3A,C). Based on TEM, e-NBs have a diameter between 90 and 250 nm (Figure 3B). With the lower limit of detection of the RMM,  $\approx 100$  nm, we can assume that the mean size and concentration measured are underestimated, since the smaller population of e-NBs formed will not be counted. In the case of v-NBs, the observed size range was from 100 to 550 nm (Figure 3D). TEM results are in agreement with RMM with e-NBs having a smaller size range than v-NBs. Moreover, 9 of the 13 bins of the e-NBs histogram (Figure 3D) represent 8% or more of the total population however only 1 under the 32 bins of the v-NBs histogram (Figure 3B) corresponding to 8%. These results further confirm that the extruder method is a promising technique for the formation of monodisperse NBs.

The acoustic response of NBs in aqueous solution (PBS) was evaluated in a custom-made “T”-shaped agarose hydrogel phantom with nonlinear contrast imaging mode using a commercial ultrasound scanner at 12 MHz (Figure 4A). This setup allowed the transducer to be in direct contact with the bubble solution. The solution was agitated using a stir bar at the bottom of the phantom, out of the imaging field. e-NB and v-NB concentrations were normalized to the same theoretical gas volume calculated from the RMM measurements. The results show that v-NBs yield a higher initial acoustic response, in the three regions of interest, Z1, Z2, and Z3, with  $30 \pm 1$  dB compared to  $17 \pm 5$  dB for e-NBs for region Z2, the area at the focal point (Figure 4B,C; average of triplicate measurement is represented by the solid line and the standard deviation is indicated with the shaded bounds). For e-NBs signal was primarily apparent in the area at the focal zone compared

to v-NBs where significant activity was also seen above and below the focus. For e-NBs signal in Z2 represents  $65 \pm 10\%$  of total region of interest (ROI) compared to  $48 \pm 1\%$  for v-NBs (Figure S2, Supporting Information). This result suggests a strong pressure-dependent acoustic response of both NB types, which, as predicted, becomes more apparent with a more monodisperse bubble population.<sup>[42,43]</sup> A smaller NB size predictably contributes to lower acoustic activity from the e-NBs at the same imaging pressures (mechanical index of 0.22), despite a comparable gas volume. In addition, the stability of the agent in the acoustic field is somewhat lower for the e-NBs. After 8 min of continuous data acquisition at 1 frame per second, minimal signal decay was observed for v-NBs. For e-NBs a 50% decay of the initial signal was observed from  $17 \pm 5$  to  $8 \pm 5$  dB (Figure 4C). However, as described above, monodispersity of bubble populations may be desired to yield a uniform acoustic signal, which can be valuable for precise imaging and focused therapy with minimized off target effects. Despite the faster decay under ultrasound exposure, the acoustic response of e-NBs is considerably more localized, which can have a strong appeal for precision diagnostic and theranostic applications.

## 2.2. Impact of Extruder Parameters

### 2.2.1. Temperature

Temperature is a critical parameter which needs to be controlled during extrusion. We examined NB formulation at 50, 65, and 80 °C to determine the optimal parameter for formulation of buoyant particles and assessed the effect of

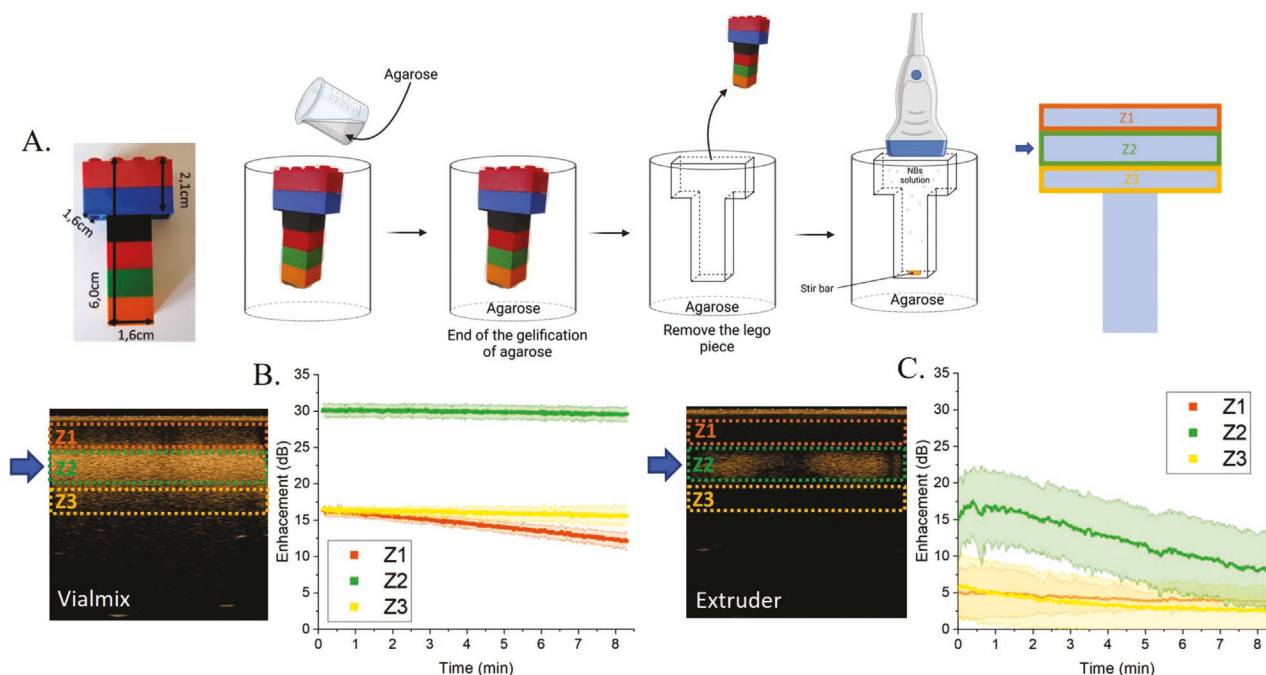


**Figure 4.** A) Preparation of the Lego-based phantom used for acoustic evaluation of NBs and the US image acquisition set up including the three regions of interest which were measured to assess the pressure-dependent activity of NB solutions. The US focus is indicated by the blue arrow. Contrast harmonic images (12 MHz, MI: 0.22) at  $t = 0$  (left) and representation of the enhancement over 8 min (right) of v-NBs B) and e-NBs C) (solid line indicates mean signal, shaded regions refers to standard deviation). Panel (A) created with BioRender.

temperature on e-NB size, yield, and ultrasound signal intensity over 8 min. At 65 °C resulting e-NB had the smallest diameter, highest concentration, and strong acoustic activity (Figure 5). Further increasing the temperature to 80 °C resulted in a decreased bubble concentration (from  $6.2 \pm 1.8 \times 10^{10}$  at 65 °C to  $1.4 \pm 1.3 \times 10^8$  e-NBs mL<sup>-1</sup> at 85 °C, Figure 5A) and a significant drop in acoustic activity in the focal zone from  $17 \pm 5$  dB at 65 °C to  $4 \pm 1$  dB at 80 °C (Figure 5C). The data suggest that 80 °C is ideal to form nonbuoyant particles because it is higher than the transition temperature of the phospholipids

used in the formulation. Lowering the temperature to 50 from 65 °C, also resulted in a decrease in bubble concentration due to a reduction in the fluidity of the phospholipid solution, but an increase in bubble diameter. Reducing the fluidity of the phospholipid solution, in turn, reduces the efficiency of the formation of foam and consequently, the formation of the NBs. Interestingly, the acoustic response at 50 °C is comparable to the one performed at 65 °C with  $21 \pm 4$  and  $17 \pm 5$  dB, respectively (Figure 5C). This suggests that bubbles produced at 50 °C to provide a significant acoustic response, potentially

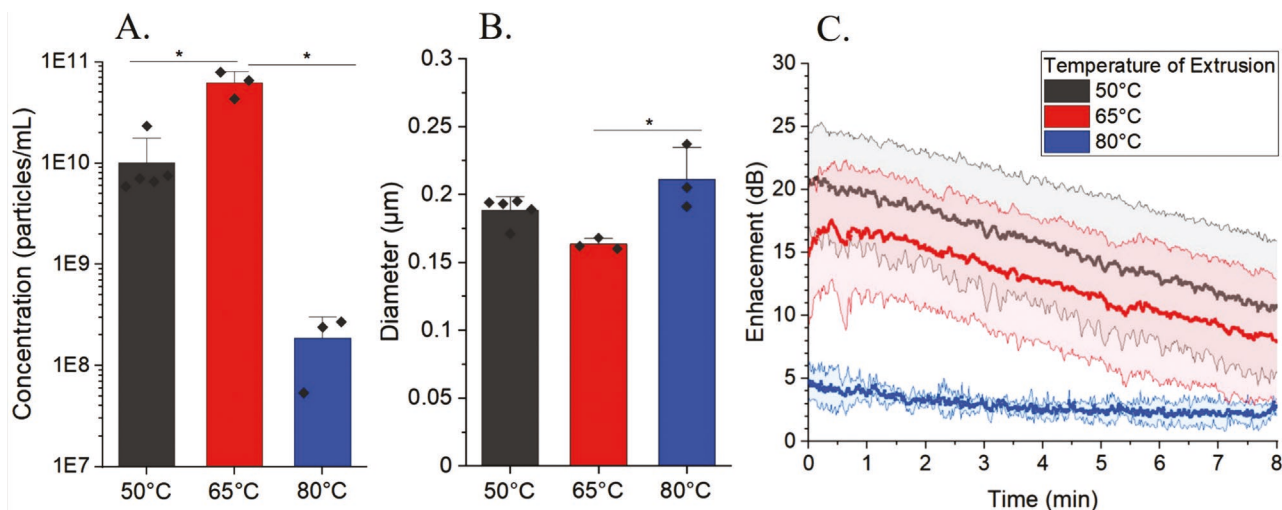


**Figure 5.** Physical and acoustic characterization of the buoyant particle population of e-NBs prepared using different temperatures: A) Total concentration, B) mean diameter, and C) representation of enhancement of Z2 over 8 min as function of the temperature of extrusion, 50 °C (black), 65 °C (red), and 80 °C (blue) (solid line indicates mean signal, shaded regions refers to standard deviation). Asterisk indicates significant difference at  $p < 0.05$ .

due to their larger diameter. For 50 and 80 °C the sizes of the NBs were  $0.19 \pm 0.01$  and  $0.21 \pm 0.02$   $\mu\text{m}$ , respectively, which is higher compared to 65 °C at  $0.16 \pm 0.004$   $\mu\text{m}$  (Figure 5B). As with lipid nanoparticle formulation, temperature is a crucial factor in forming an efficient NBs. Temperature affects the fluidity of the solution, which is critical to efficiency pass the solution through the extruder without producing liquid-core self-assembly. A temperature higher than the transition phase of the PL, corresponding to 80 °C here, will result in the formation of more nonbuoyant particles. On the contrary, if the temperature is too low, here at 50 °C, the lipids are not fluid enough to easily pass through the 0.8  $\mu\text{m}$  membrane. 65 °C resulted in a solution fluid enough to pass through the extruder without reaching the transition phase of all PL.

### 2.2.2. Lipid Concentration

Using mechanical agitation followed by centrifugation and filtration to produce monodisperse NBs can result in significant starting material loss of ( $\approx 50\%$ ). Initially, a highly polydisperse bubble population is formed, and upon isolation of NBs, from the solution, a significant portion of the lipids is discarded. Further changes to the technique along with adjustments to the dilution can be implemented to help reduce material loss and improve process efficiency. Here we examined the effect phospholipid (PL) concentration on e-NB formulation. The standard v-NBs formulation consists of 10 mL solution at 10 mg mL<sup>-1</sup> of PL dilute in a mixture of PG, Gly, and PBS. In these experiments PL concentrations of 2 mg mL<sup>-1</sup> (20:80), 5 mg mL<sup>-1</sup> (50:50), 7 mg mL<sup>-1</sup> (70:30), and 10 mg mL<sup>-1</sup> (100:0), in the same mixture of solvent, were also investigated. Results show that decreasing the PL concentration has a significant impact on the NB concentration, size, and acoustic response (Figure 6). Low PL concentrations result in low e-NB yield and an increase in NB size (from  $0.21 \pm 0.05$   $\mu\text{m}$  for 2 mg mL<sup>-1</sup> to  $0.160 \pm 0.004$   $\mu\text{m}$  for 7 mg mL<sup>-1</sup>, Figure 6B). This observation is similar to previous reports using microfluidic bubbles wherein a decrease in the proportion of PL

in the solution generated very unstable bubbles, which tend to coalesce more easily.<sup>[44]</sup> At 5 mg mL<sup>-1</sup> the NB concentration was significantly lower ( $1.5 \pm 0.8 \times 10^{10}$  e-NBs mL<sup>-1</sup>) than at 7 mg mL<sup>-1</sup> ( $6.2 \pm 1.8 \times 10^{10}$  e-NBs mL<sup>-1</sup>), while a ratio of 10 mg mL<sup>-1</sup> was slightly lower ( $5.4 \pm 0.6 \times 10^{10}$  e-NBs mL<sup>-1</sup>). Despite these changes in concentration the ultrasound signal for each ratio was unchanged with the exception of the lowest PL concentration ( $17 \pm 5$  vs  $5 \pm 3$  dB, respectively, Figure 6C). Ultimately we selected, the 7 mg mL<sup>-1</sup> ratio was used for the optimized protocol.

### 2.2.3. Number of Extruder Passes

The number of passes through the extruder influences the polydispersity of resulting nanoparticles. An increase in the number of times the solution passes through the extruder typically leads to more monodisperse vesicles or liposomes.<sup>[45]</sup> In our experiments, we examined a range of 10–40 passes. Surprisingly, no significant differences were observed in e-NB properties (Figure 7). The concentration slightly increased comparing 10-pass to 30-pass samples from  $2.5 \pm 0.5 \times 10^{10}$  to  $6.2 \pm 1.8 \times 10^{10}$  e-NBs mL<sup>-1</sup> and then decreased for the 40-pass samples. This suggests that the majority of e-NBs are formed in the first steps of the extrusion process. This was also confirmed by comparable acoustic response for the different number of passes used (Figure 7C). In the case of the e-NBs, the monodispersity of the samples was improved by the removal of bigger bubbles with the combination of centrifugation and the use of a 0.45  $\mu\text{m}$  polyethersulfone (PES) membrane filter following extrusion. However, based on these results, 30 passes can be chosen as the optimal protocol used to produce bubbles with a smaller size, high yield, and a good acoustic response.

### 2.3. In Vivo Assessment of e-NBs

For the purpose of demonstrating in vivo activity, a variation of e-NB protocol was developed to achieve a significantly higher

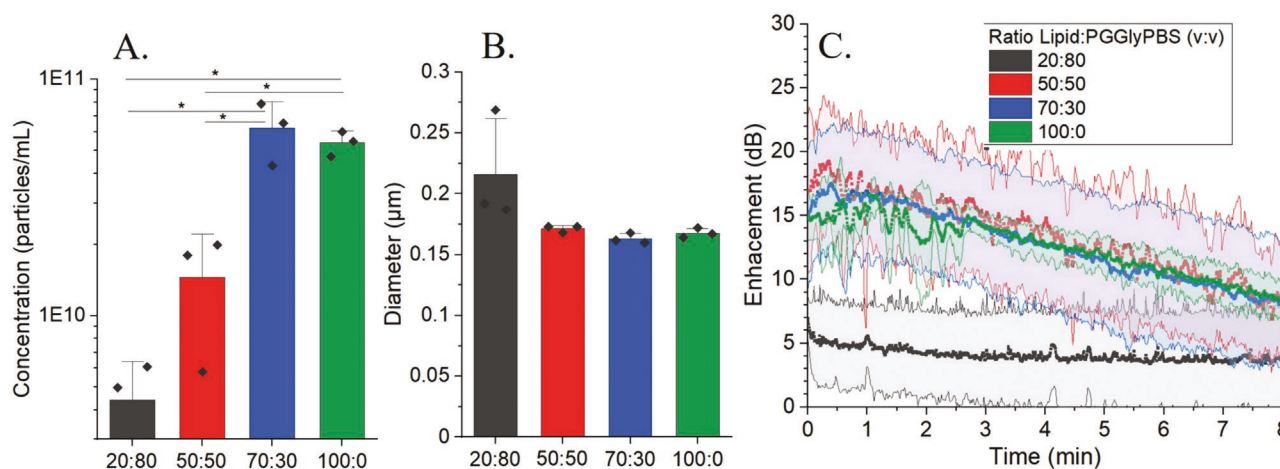


**Figure 6.** Physical and acoustic characterization of the buoyant particle population of e-NBs prepared using different ratios of lipids and surfactants: A) Total concentration, B) mean diameter, and C) Acoustic response time intensity curve showing enhancement in Z2 region over 8 min ( $n = 3$ ) (solid line indicates mean signal, shaded regions refers to standard deviation). Asterisk indicates significant difference at  $p < 0.05$ .

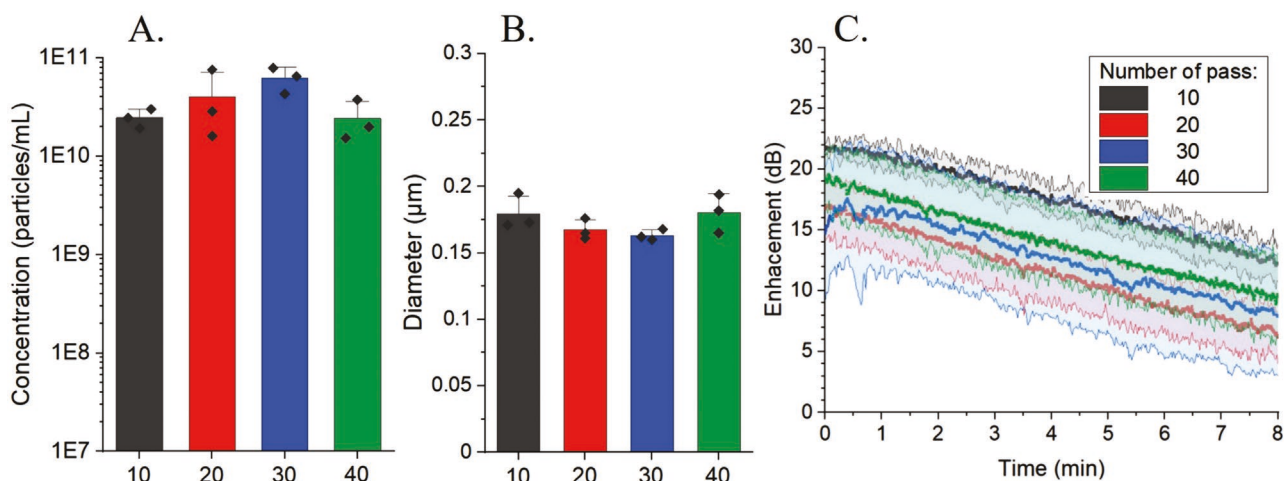


**Figure 7.** Physical and acoustic characterization of the buoyant particle population of e-NBs prepared using different number of passes: A) Total concentration, B) mean diameter, and C) representation of enhancement of Z2 over 8 min as function of the pass number through the extruder, 10 (black), 20 (red), 30 (blue), and 40 (green) (solid line indicates mean signal, shaded regions refers to standard deviation). Asterisk indicates significant difference at  $p < 0.05$ .

response from in vivo imaging. Here, after the extrusion, the resulting NB solution was directly passed through a 0.8 μm mixed cellulose ester (MCE) filter and centrifugation was omitted (Figure S5, Supporting Information).

Because of their small size and monodispersity, e-NBs require higher acoustic pressures for generating nonlinear activity (on which the contrast enhanced ultrasound sequences depend) which would not be practical for in vivo studies. As shown previously,<sup>[43]</sup> a reduction in size on nanobubbles by a factor of 2 more than doubles the pressure threshold for nonlinear activity. Therefore, when the mean size is shifted from 160 to 200 nm, the bubbles can be visualized in vivo with the same pressure and frequency as the v-NB (Figures S1 and S3, Supporting Information).

The resulting in vivo e-NBs, had a size of ≈200 nm, with a similar distribution as the optimal e-NBs. Their in vitro acoustic response was also very similar to those of the v-NBs (Figure S1, Supporting Information). e-NBs were evaluated in healthy mice upon injection into the tail vein. Bubbles were normalized based on theoretical gas volume prior to injection.

In vivo, the acoustic enhancement in the kidney (K) and the liver (L) of mice was measured for both v-NBs and e-NBs. The e-NBs had a lower initial peak response than v-NBs, with  $9 \pm 2$  dB compared to  $13 \pm 8$  dB, respectively, for the liver (Figure 8A) and  $13 \pm 2$  dB compared to  $17 \pm 4$  dB, respectively, for the kidney (Figure 8B). The response of in vivo e-NBs decreased at a higher rate than the v-NBs. This faster decay of in vivo e-NBs was likely a result of the smaller bubble size and improved monodispersity because of the sensitive dependence of acoustic response to NB diameter.<sup>[46]</sup>

A comparison of the enhancement within the different imaging zones showed differences above and under the focus versus the focus area for the 2 bubbles categories. The focus region consistently yielded the highest enhancement. However, the average percentage of the focus zone compared to the global region of interest of the kidney from 30 s to 10 min is  $56 \pm 16\%$  for e-NBs compared to  $46 \pm 12\%$  for v-NBs (Figure S4,

Supporting Information). This is consistent with the in vitro experiment. These results illustrate that, while attractive for various application, monodisperse bubbles may not be ideal for some in vivo imaging applications, where pressures can vary tremendously. Likewise, as discussed above, a faster decay of monodisperse nanobubbles was seen, which could also be driven by uniform decay in the acoustic field compared to the less-uniform decay of polydisperse formulations. Recent work demonstrated a unique microfluidic approach to formulate uniform NBs, by the formation of N<sub>2</sub>/C<sub>3</sub>F<sub>8</sub> MBs, which became NBs by dissolution of N<sub>2</sub> with time within the microfluidic reservoir.<sup>[32]</sup> The obtained NB population using this method is of similar size scale as the e-NB, but a 100–1000 times lower concentration compared to the technique presented here (10<sup>7</sup> vs 10<sup>10</sup>). The acoustic activity of the microfluidic NBs in vivo was shown for NBs that were greater than 300 nm in diameter. The same NBs were imaged in vivo for 20 s, with signal decay starting after 10 s. Importantly, the polydispersity can be tuned according to the ultimate application with simple modifications to the extrusion setup. Further specific modifications can be investigated in future applications to optimize extruded nanobubbles for diagnostic or therapeutic applications.

### 3. Conclusion

We have demonstrated, for the first time, the possibility of creating gas core self-assembly using a standard mini-extruder setup, which was previously used exclusively to form non-buoyant, liquid-core agents. The high yield e-NBs produced featured a smaller size and reduced polydispersity compared to NBs formed by mechanical agitation. We also demonstrated that the e-NBs have a more focused acoustic response, critical for ultrasound targeted drug delivery applications. The extrusion process is a complex mechanism where multiple parameters can impact the result of NBs formation. Temperature and lipid concentration are the two main factors that

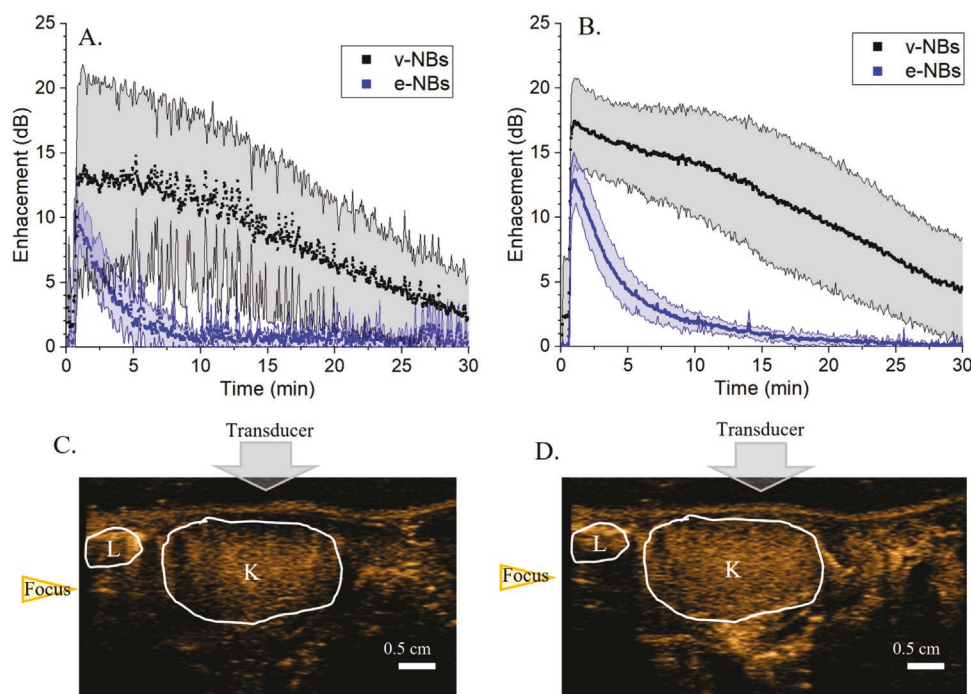


**Figure 8.** In vivo contrast ultrasound signal enhancement time intensity curves for A) Liver (L) and B) kidney (K) for v-NB and e-NBs over 30 min with NB injection starting at 30 s (12 MHz, MI:0.2). Representative contrast harmonic images of in vivo e-NBs (C) and v-NBs (D) at  $t = 1$  min (solid line indicates mean signal, shaded regions refers to standard deviation).

contribute to formation of small NBs with a high yield using the extrusion process. The temperature must be optimized to provide a good balance between the ability of the solution to cross the membrane without leading to the formation of non-buoyant vesicles, as determined by the fluidity of the solution. In terms of PL concentration, optimization can determine the minimum PL concentration needed to avoid the potential for bubble coalescence at low PL concentrations, and shear forces with increasing PL concentration.<sup>[44]</sup> Overall, the extrusion technique presented here shows promise for simple, efficient, and cost-effective NB production, with potential for straightforward scale up using existing strategies. Testing the extruded NBs in the biomedical imaging application showed feasibility of these particles as contrast agents with a strong and stable acoustic response, which is highly pressure dependent. The first in vivo study using extrusion produced NBs also showed significant signal enhancement in mouse kidney within the focal zone for an extended time. Additional optimization of the formulation and image acquisition parameters can yield a further improved imaging and therapeutic response.

#### 4. Experimental Section

**Raw Materials:** Phospholipids (PL) including DBPC (1,2-dibehenoyl-*sn*-glycero-3-phosphocholine), DPPA (1,2 dipalmitoyl-*sn*-glycero-3-phosphate), and DPPE (1,2-dipalmitoyl-*sn*-glycero-3-phosphoethanolamine) were obtained from Avanti Polar Lipids (Pelham, AL), and mPEG-DSPE (1,2-distearoyl-*sn*-glycero-3-phosphoethanolamine-*N*-[methoxy(polyethylene glycol)-2000] (ammonium salt)) was obtained from Laysan Lipids (Arab,AL). Propylene glycol (PG) was purchased from Sigma. Glycerol was purchased from Acros Organics (Morris, NJ).

Octafluoropropane was obtained from AirGas (Cleveland, OH). Sterile PES syringe filter, 0.45  $\mu\text{m}$  pore size, 30 mm and sterile MCE syringe filter, 0.8  $\mu\text{m}$  pore size, 33 mm, were purchased from Celltreat and Millipore, respectively.

**Fabrication of Mechanical Agitation Nanobubbles (v-NBs):** Mechanical agitation formulation of lipids shelled v-NBs stabilized with octafluoropropane ( $\text{C}_3\text{F}_8$ ) has been described previously.<sup>[20]</sup> Briefly, lipids including DBPC (60.1 mg), DPPA (10 mg), DPPE (20 mg), and mPEG-DSPE (10 mg) were dissolved in propylene glycol (PG) (1 mL). 9 mL of a mixture of glycerol (Gly) and PBS (1:8, v:v) was added to the lipid solution after dissolution of the PL at 80 °C. In a sealed 3 mL vial, the lipid solution (1 mL) was added and the air inside was replaced with  $\text{C}_3\text{F}_8$ . Finally, the vial was placed on a VialMix shaker (Bristol-Myers Squibb Medical Imaging, Inc., N. Billerica, MA) for 45 s to drive bubble self-assembly. v-NBs were isolated from the mixture by centrifugation at 50 rcf for 5 min with the vial inverted. 500  $\mu\text{L}$  v-NBs were obtained from the vial.

**Fabrication of Extruder Nanobubbles (e-NBs):** Extruder formulation of lipid shelled e-NBs stabilized with octafluoropropane ( $\text{C}_3\text{F}_8$ ) were made from the same lipid solution mixture as mechanical agitation formulation v-NBs previously described.<sup>[20]</sup> Briefly, lipids including 60.1 mg of DBPC, 10 mg of DPPA, 20 mg of DPPE, and 10 mg of mPEG-DSPE were dissolved in 1 mL of propylene glycol (PG). 9 mL of a mixture of glycerol and PBS (1:8, v:v) was added to the lipid solution after dissolution of the PL at 80 °C. This lipid solution (7 mL) was then diluted with PG:Gly:PBS (1:1:8 v:v:v) mixture (3 mL). In a sealed 3 mL vial, the dilute lipid solution (1 mL) was added and the air inside was replaced with  $\text{C}_3\text{F}_8$ . A mini-extruder from Avanti Polar Lipid, well known for the formulation of liposomes/vesicles, was used to make the e-NBs. The extruder was set-up with a 0.8  $\mu\text{m}$  pore diameter polycarbonate membrane. Lipid solutions of 2, 5, 7  $\text{mg mL}^{-1}$  (e-NBs reference concentration) and 10  $\text{mg mL}^{-1}$  (v-NBs reference concentration) were tested. Before starting the extrusion process, the system (syringe and extruder) was equilibrated to the appropriate temperature (50–80 °C) for 10 min. The solution was passed through the extruder 10–40 times. At the end of the extrusion process, the empty syringe was removed and the solution was passed

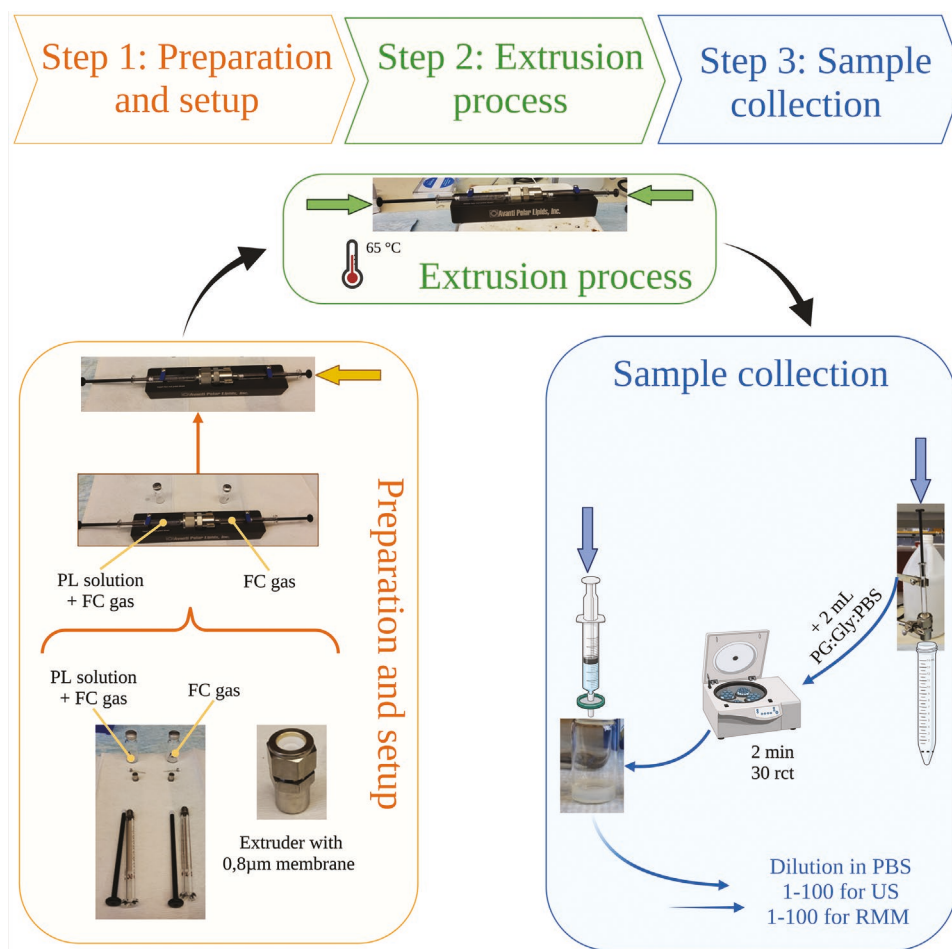


**Figure 9.** Schematic showing the preparation of nanobubbles using the mini-extruder. The extruder was outfitted with a 0.8 μm membrane. Syringes provided by Avanti are filled with lipid solution and FC gas, connected to the extruder and heated to the desired temperature on the heat block. For the extrusion, the mixture is passed 30 times through the extruder membrane. Following the extrusion process, the contents are emptied into a 15 mL tube, syringes are rinsed with the desired solvent, and all material is collected. The mixture is centrifuged for 2 min at 30 rcf and passed through a 0.45 μm PES filter. If preparing for imaging, the centrifugation step is omitted and the solution is passed through a 0.8 μm PES filter to remove foam. Created with BioRender.

for the last time through the extruder for collection in a 15 mL falcon tube. Both syringes were then washed with PG:Gly:PBS. Centrifugation at 30 rcf for 2 min was used to quickly discard the foam formed during the extrusion process. The liquid part was then passed through a 0.45 μm PES membrane filter. Between 2.5 and 3 mL of e-NBs solution was obtained after filtration (Figure 9).

For in vivo measurement, the e-NBs production protocol was modified. Here, after the extrusion and washing process the formulation was directly passed to a sterile MCE syringe filter of 0.8 μm pore size without centrifugation. This modification allowed to prepare NBs which gave significant contrast under in vivo conditions.

**Characterization of NB Morphology, Size, and Concentration—RMM:** The size distribution, concentration, and buoyant mass of NBs were measured using RMM (Archimedes, Malvern Pananalytical Inc., Westborough, MA) using a calibrated nanosensor (100 nm–2 μm).<sup>[41]</sup> Sensors were precalibrated using NIST traceable 565 nm polystyrene bead standards (ThermoFisher 4010S, Waltham MA). E-NBs and v-NBs were diluted 1:100 and 1:1000, respectively, with PBS (pH 7.4) before measurement. A total of 500 particles were measured for each trial ( $n \geq 3$ ). The SD is the one of the trials only.

**Characterization of NB Morphology, Size, and Concentration—TEM:** Bubble morphology was imaged with a TEM (Tecnai G2 Spirit BioTWIN, FEI Company) operated at 120 kV based on a previously reported

method (Owen and Stride, 2015). 10 μL of a dilute suspension of v-NBs and e-NBs, at 1:100 and 1:10 dilution, respectively, were placed in an inverted position for 2 min on a 400 mesh Formvar-coated copper grid. The sample was then stained by placing it on top of a 20 μL droplet of 2% uranyl acetate for 30 s and the excess was removed. The TEM grid containing the bubble sample was allowed to dry for another 30 min.

**Characterization of NB Morphology, Size, and Concentration—Stability Under Ultrasound:** Stability under ultrasound was studied in a “T” agarose phantom (Figure 4D) with an ultrasound transducer (PLT-1204BT) placed directly on the top, in contact with the phantom and the media. The phantom was filled with a total of 20 mL of certain volume of e-NBs or v-NBs dispersion in PBS. For the controlled e-NBs and v-NBs comparison, NBs were diluted in PBS to satisfy a matched 0.02 μL gas volume. However, for the evaluation of the extruder parameters the dilution of e-NBS in PBS was fixed at 1:100 dilution. In all cases, the solution was stirred at 700 rpm through the full duration of imaging acquisition. Before starting the acquisition, the solution was stirred at 1000 rpm for 10 s to reach an approximately homogenous distribution of NBs throughout the imaging plane. Nonlinear contrast images were continuously acquired using a clinical US scanner (AplioXG SSA-790A, Toshiba Medical Imaging Systems, Otawara-Shi, Japan) via contrast harmonic imaging (CHI, 12 MHz, mechanical index 0.22, focus depth of 0.75 cm, 2D gain of 70 dB, dynamic range of 65 dB) at 1 frame per second

for 8 min. Raw echo power data were recorded and analyzed using a built-in CHI-Q software. Images were analyzed using quantification software (CHI-Q) available on the scanner. Using the software, the mean intensity of the backscattered nonlinear ultrasound signal over time was measured in selected regions of interest, and these values were used to create the time intensity curves (TIC). For the in vitro data to quantify the extent of pressure dependent NB activity, the signal was measured in 3 zones (Z1 above the focus, Z2 at the focus, and Z3 below the focus). For each zone, the background signal was subtracted prior to constructing the TIC. Signal decay over time was determined from this data (Figure 4). Experiments were repeated in triplicate.

**Characterization of NB Morphology, Size, and Concentration—In Vivo Ultrasound Imaging:** Mice were handled according to a protocol approved by the Institutional Animal Care and Use Committee (IACUC) at Case Western Reserve University and were in accordance with all applicable protocols and guidelines in regards to animal use (CWRU IACUC protocol number 2016-0024). Male athymic nude mice (4–6 weeks old) were anesthetized with inhalation of 2% isoflurane (100 mL min<sup>-1</sup> air). Tail vein administration of 200 μL of undiluted in vivo e-NBs (0.8 μm filter e-NBs described previously), or diluted to the same gas volume v-NBs, were performed. The same US probe as above was placed to visualize kidney and liver. Contrast harmonic imaging (CHI, frequency, 12.0 MHz; MI, 0.2; dynamic-range, 65 dB; gain, 70 dB; imaging frame rate, 0.2 frames s<sup>-1</sup>) was used to determine the change of tissue contrast during a 30 min imaging period. At least 3 flash replenish pulses (high energy pulses) were done between e-NBs and v-NBs measurements, to remove the remaining NBs. After 30 min of waiting time other type of bubble injected. Raw echo power data was recorded and was again analyzed using a built-in CHI-Q software as described above. Signal decay over time was determined from the data. The kidney and liver area was delineated by drawing regions of interest. The experiments were carried out in triplicate.

**Statistical Analysis:** All experiments were carried out with minimum of triplicates, and the results were reported as mean ± standard deviation (SD). One-way ANOVA with Tukey's multiple comparisons was carried out using Origin Lab to compare the means. Statistical significance was recorded as \**p* < 0.05.

## Supporting Information

Supporting Information is available from the Wiley Online Library or from the author.

## Acknowledgements

The authors would like to acknowledge funding and support for this study from the Case-Coulter Translational Research Partnership and Wallace H. Coulter Foundation. This work was also supported by the National Institutes of Health via the National Institute of Biomedical Imaging and Bioengineering (NIBIB) under Award No. R01EB028144. We also appreciate the many spirited discussions on this topic with Dr. Kolios and Dr. Sojahrood. Dana Wegierak was of great help for correction and organization of this paper.

## Conflict of Interest

The authors declare no conflict of interest.

## Author Contributions

E.A. performed the TEM experiments and R.P. performed the in vivo experiments.

## Data Availability Statement

The data that support the findings of this study are available from the corresponding author upon reasonable request.

## Keywords

contrast-enhanced ultrasound, extrusion, monodispersity, nanobubbles

Received: February 7, 2022

Revised: April 24, 2022

Published online: May 19, 2022

- [1] R. Gramiak, P. M. Shah, *Invest. Radiol.* **1968**, *3*, 356.
- [2] A. A. Exner, M. C. Kolios, *Curr. Opin. Colloid Interface Sci.* **2021**, *54*, 101463.
- [3] L. Pociavsek, K. Gavrillov, K. D. Cao, E. Y. Chi, D. Li, B. Lin, M. Meron, J. Majewski, K. Y. Lee, *Biophys. J.* **2011**, *101*, 118.
- [4] X. Wang, H. Chen, K. Zhang, M. Ma, F. Li, D. Zeng, S. Zheng, Y. Chen, L. Jiang, H. Xu, J. Shi, *Small* **2014**, *10*, 1403.
- [5] K. P. Hadinger, J. P. Marshalek, P. S. Sheeran, P. A. Dayton, T. O. Matsunaga, *Ultrasound Med. Biol.* **2018**, *44*, 2728.
- [6] J. D. Rojas, P. A. Dayton, *Ultrasound Med. Biol.* **2019**, *45*, 177.
- [7] A. G. Nyankima, J. D. Rojas, R. Cianciolo, K. A. Johnson, P. A. Dayton, *Ultrasound Med. Biol.* **2018**, *44*, 368.
- [8] Z. Zha, S. Wang, S. Zhang, E. Qu, H. Ke, J. Wang, Z. Dai, *Nanoscale* **2013**, *5*, 3216.
- [9] F. Dong, J. Zhang, K. Wang, Z. Liu, J. Guo, J. Zhang, *Nanoscale* **2019**, *11*, 9216.
- [10] Y. Xie, J. Wang, Z. Wang, K. A. Krug, J. D. Rinehart, *Nanoscale* **2018**, *10*, 12813.
- [11] B. B. Goldberg, J. B. Liu, F. Forsberg, *Ultrasound Med. Biol.* **1994**, *20*, 319.
- [12] B. A. Kaufmann, J. R. Lindner, *Curr. Opin. Biotechnol.* **2007**, *18*, 11.
- [13] M. A. Borden, H. Zhang, R. J. Gillies, P. A. Dayton, K. W. Ferrara, *Biomaterials* **2008**, *29*, 597.
- [14] E. G. Schutt, T. J. Pelura, R. M. Hopkins, *Acad. Radiol.* **1996**, *3*, S188.
- [15] F. Yang, S. Hu, Y. Zhang, X. Cai, Y. Huang, F. Wang, S. Wen, G. Teng, N. Gu, *Adv. Mater.* **2012**, *24*, 5205.
- [16] P.-L. Lin, R. J. Eckersley, E. A. H. Hall, *Adv. Mater.* **2009**, *21*, 3949.
- [17] H. Y. Huang, H. L. Liu, P. H. Hsu, C. S. Chiang, C. H. Tsai, H. S. Chi, S. Y. Chen, Y. Y. Chen, *Adv. Mater.* **2015**, *27*, 655.
- [18] Y. Zhou, Z. Wang, Y. Chen, H. Shen, Z. Luo, A. Li, Q. Wang, H. Ran, P. Li, W. Song, Z. Yang, H. Chen, Z. Wang, G. Lu, Y. Zheng, *Adv. Mater.* **2013**, *25*, 4123.
- [19] E. Y. Lukianova-Hleb, X. Ren, J. A. Zasadzinski, X. Wu, D. O. Lapotko, *Adv. Mater.* **2012**, *24*, 3831.
- [20] A. de Leon, R. Perera, C. Hernandez, M. Cooley, O. Jung, S. Jeganathan, E. Abenojar, G. Fishbein, A. J. Sojahrood, C. C. Emerson, P. L. Stewart, M. C. Kolios, A. A. Exner, *Nanoscale* **2019**, *11*, 15647.
- [21] R. H. Perera, A. de Leon, X. Wang, Y. Wang, G. Ramamurthy, P. Peiris, E. Abenojar, J. P. Babilion, A. A. Exner, *Nanomedicine* **2020**, *28*, 102213.
- [22] R. G. Maheshwari, R. K. Tekade, P. A. Sharma, G. Darwhekar, A. Tyagi, R. P. Patel, D. K. Jain, *Saudi Pharm. J.* **2012**, *20*, 161.
- [23] G. M. El Maghraby, B. W. Barry, A. C. Williams, *Eur. J. Pharm. Sci.* **2008**, *34*, 203.
- [24] A. C. Biondi, E. A. Disalvo, *Biochim. Biophys. Acta, Biomembr.* **1990**, *1028*, 43.
- [25] E. C. Abenojar, P. Nittayacharn, A. C. de Leon, R. Perera, Y. Wang, I. Bederman, A. A. Exner, *Langmuir* **2019**, *35*, 10192.

- [26] W. Terakosolphan, J. L. Trick, P. G. Royall, S. E. Rogers, O. Lamberti, C. D. Lorenz, B. Forbes, R. D. Harvey, *Langmuir* **2018**, *34*, 6941.
- [27] A. J. Sojahrood, A. C. d. Leon, R. Lee, M. Cooley, E. C. Abenojar, M. C. Kolios, A. A. Exner, *ACS Nano* **2021**, *15*, 4901.
- [28] T. Segers, P. Kruizinga, M. P. Kok, G. Lajoinie, N. de Jong, M. Versluis, *Ultrasound Med. Biol.* **2018**, *44*, 1482.
- [29] R. L. Hall, Z. D. Juan-Sing, K. Hoyt, S. R. Sirsi, *Langmuir* **2019**, *35*, 10977.
- [30] E. Stride, T. Segers, G. Lajoinie, S. Cherkaoui, T. Bettinger, M. Versluis, M. Borden, *Ultrasound Med. Biol.* **2020**, *46*, 1326.
- [31] B. Van Elburg, G. Collado-Lara, G.-W. Bruggert, T. Segers, M. Versluis, G. Lajoinie, *Rev. Sci. Instrum.* **2021**, *92*, 035110.
- [32] J. Xu, A. Salari, Y. Wang, X. He, L. Kerr, A. Darbandi, A. C. de Leon, A. A. Exner, M. C. Kolios, D. Yuen, S. S. H. Tsai, *Small* **2021**, *17*, e2100345.
- [33] T. Segers, L. de Rond, N. de Jong, M. Borden, M. Versluis, *Langmuir* **2016**, *32*, 3937.
- [34] F. Brauns, G. Pawlik, J. Halatek, J. Kerssemakers, E. Frey, C. Dekker, *Nat. Commun.* **2021**, *12*, 3312.
- [35] M. Salvador-Castell, M. Golub, N. Erwin, B. Deme, N. J. Brooks, R. Winter, J. Peters, P. M. Oger, *Commun. Biol.* **2021**, *4*, 653.
- [36] J. Lizarrondo, D. P. Klebl, S. Niebling, M. Abella, M. A. Schroer, H. D. T. Mertens, K. Veith, R. Thuenauer, D. I. Svergun, M. Skrzuzny, F. Sobott, S. P. Muench, M. M. Garcia-Alai, *Nat. Commun.* **2021**, *12*, 2889.
- [37] H. Bi, Z. Chen, J. Qiu, *Des. Monomers Polym.* **2021**, *24*, 158.
- [38] C. M. Robert, I. M. Ruby, M. M. Bert Ph, T. Keizo, K. S. Nanda, H. Lan-rong, *Bioch. Biophys. Acta, Biomembr.* **1991**, *1061*, 297.
- [39] K. Daniel, G. Zhiliang, S. Tiffany, L. Adrienne, R. Sobhan, S. Renee, H. Hyeondo Luke, J. M. Henderson, D. C. Kathleen, B. Wei, L. Binhua, T. T. Gregory, L. S. Theodore, J. A. Erin, C. L. Ka Yee, *Biophys. J.* **2021**, *120*, 4891.
- [40] S. Keisuke, O. Tsutomu, T. Mamiko, K. Takashi, S. Hiroaki, *Chem. Phys. Lipids* **2021**, *241*, 105148.
- [41] C. Hernandez, E. C. Abenojar, J. Hadley, A. C. de Leon, R. Coyne, R. Perera, R. Gopalakrishnan, J. P. Babilion, M. C. Kolios, A. A. Exner, *Nanoscale* **2019**, *11*, 851.
- [42] A. J. Sojahrood, O. Falou, R. Earl, R. Karshafian, M. C. Kolios, *Non-linear Dyn.* **2015**, *80*, 889.
- [43] A. J. Sojahrood, R. Earl, H. Haghi, Q. Li, T. M. Porter, M. C. Kolios, R. Karshafian, *Nonlinear Dyn.* **2021**, *103*, 429.
- [44] T. Segers, D. Lohse, M. Versluis, P. Frinking, *Langmuir* **2017**, *33*, 10329.
- [45] M. B. de Jesus, A. Radaic, I. S. Zuhorn, E. de Paula, *J. Nanopart. Res.* **2013**, *15*, 1960.
- [46] S. Rossi, C. Szijjártó, F. Gerber, G. Waton, M. P. Krafft, *J. Fluorine Chem.* **2011**, *132*, 1102.